Ultrasonics Sonochemistry 88 (2022) 106075

Contents lists available at ScienceDirect

Ultrasonics Sonochemistry

journal homepage: www.elsevier.com/locate/ultson

Effects of ultrasonic pretreatment of soybean protein isolate on the binding efficiency, structural changes, and bioavailability of a protein-luteolin nanodelivery system

Fuwei Sun [a,1], Bailiang Li [a,1], Yanan Guo [a], Yichang Wang [a], Tianfu Cheng [a], Qingyu Yang [b], Jun Liu [c,d], Zhijun Fan [e], Zengwang Guo [a,*], Zhongjiang Wang [a,*]

[a] College of Food Science, Northeast Agricultural University, Harbin, Heilongjiang 150030, China
[b] College of Grain Science and Technology, Shenyang Normal University, Shenyang 110034, China
[c] Kedong Yuwang Soybean Protein Food Co., Ltd, Qiqihaer, Heilongjiang 161000, China
[d] Shandong Yuwang Industrial Co., Ltd, Dezhou, Shandong 251299, China
[e] Heilongjiang Beidahuang Green and Healthy Food Co., Ltd, Jiamusi, Heilongjiang 154007, China

ARTICLE INFO

Keywords:
Soy protein isolate
Ultrasonic
Luteolin
Nanodelivery system
Physicochemical properties

ABSTRACT

The combination of protein and flavonoids can ameliorate the problems of poor solubility and stability of flavonoids in utilization. In this study, soybean protein isolate pretreated by ultrasonication was selected as the embedding wall material, which was combined with luteolin to form a soybean protein isolate-luteolin nanodelivery system. The complexation effect and structural changes of soybean protein isolate (SPI) and ultrasonic pretreatment (100 W, 200 W, 300 W, 400 W and 500 W) of soybean protein isolate with luteolin (LUT) were compared, as well as the changes in digestion characteristics and antioxidant activity in vitro. The results showed that proper ultrasonic pretreatment increased the encapsulation efficacy, loading amount and solubility to 89.72%, 2.51 μg/mg and 90.56%. Appropriate ultrasonic pretreatment could make the particle size and the absolute value of ζ-potential of SPI-LUT nanodelivery system decrease and increase respectively. The FTIR and fluorescence results show that appropriate ultrasonic pretreatment could reduce α-helix, β-sheet and random coil, increase β-turn, and enhance fluorescence quenching. The thermodynamic evaluation results indicate that the $\Delta G < 0$, $\Delta H > 0$ and $\Delta S > 0$, so the interaction of LUT with the protein was spontaneous and mostly governed by hydrophobic interactions. The XRD results show that the LUT was amorphous and completely wrapped by SPI. The DSC results showed that ultrasonic pretreatment could improve the thermal stability of SPI-LUT nanodelivery system to 112.66 ± 1.69 °C. Digestion and antioxidant analysis showed that appropriate ultrasonic pretreatment increased the LUT release rate and DPPH clearance rate of SPI-LUT nanodelivery system to 89.40 % and 55.63 % respectively. This study is a preliminary source for the construction of an SPI nanodelivery system with ultrasound pretreatment and the deep processing and utilization of fat-soluble active substances.

1. Introduction

Luteolin is a natural flavonoid that widely exists in celery, green pepper, broccoli, carrot, perilla leaf, Ganju tea and other vegetables and Chinese herbal medicines[21]. Due to the O-dihydroxy structure in the luteolin B ring, luteolin has a strong free radical capture ability, which provides good antioxidant capacity[3]. However, due to its poor water solubility, easy decomposition under light and low bioavailability, its processing and application are greatly limited. To expand the physicochemical steadiness and water solubility of luteolin, the transport of luteolin by different kinds of substances has been studied, such as cyclodextrin-embedding complexes, phospholipid complexes, copolymer micelles and solid lipid nanoparticles[14,30,44,46]. Although the encapsulation effect is good, there are some problems, such as complex processing technology and unsuitable industrial production. Research shows that plant-based proteins can be directly used as carriers of fat-soluble active substances, to improve the solubility and bioavailability of fat-soluble active substances, improve the stability under adverse

* Corresponding authors.
E-mail addresses: gzwname@163.com (Z. Guo), wzjname@126.com (Z. Wang).
[1] These authors contributed equally to this work.

https://doi.org/10.1016/j.ultsonch.2022.106075
Received 16 May 2022; Received in revised form 8 June 2022; Accepted 17 June 2022
Available online 22 June 2022
1350-4177/© 2022 The Author(s). Published by Elsevier B.V. This is an open access article under the CC BY-NC-ND license (http://creativecommons.org/licenses/by-nc-nd/4.0/).

environmental factors such as oxygen or ultraviolet radiation, and mask the unique smell of natural phenols Dai et al. [12]. In addition, protein-based carriers can be used to effectively control the release of bioactive substances and the degradation sites of controlled particles. However, their delivery efficiency is affected by the protein structure[38].

SPI is a traditional food additive that is rich in essential amino acids such as Lys and Glu acids. The amino acid configuration of SPI is comparable to that of humans in hereditary assembly, and SPI is considered to be the most nutritious and valuable protein[19]. In aqueous solution, natural SPI has amphiphilic groups and good water solubility as a carrier wall material. The hydrophobic region in soybean protein is the active region that binds fat-soluble polyphenols. However, due to the spherical structure, the hydrophobic region is wrapped inside, so it cannot carry polyphenols. Therefore, Ultrasonic prehandling of natural SPI is helpful to extend the protein structure, disconnect the chemical bond between protein peptide chains, destroy the close relationship between molecules or within molecules, and expose more hydrophobic areas [6,50]. However, the interaction mechanism of soybean protein as a plant-based carrier of luteolin is not clear, and the impact of ultrasonic prehandling on the construction and bioavailability of the plant protein lipid-soluble active material nanosystem is not clear.

Therefore, the SPI was modified by ultrasonic pretreatment, and a SPI-LUT nanodelivery system was constructed. By characterizing the encapsulation effect (encapsulation efficacy, loading amount, solubility), morphology (particle size, ζ-potential, atomic force microscope), structure (endogenous fluorescence spectrum, Fourier transform infrared spectrum, DSC, XRD, surface hydrophobicity) to explore the interaction between soybean protein isolate and luteolin and the mechanism of a nanodelivery system, we evaluated the bioavailability of the nanodelivery system by considering the digestion and oxidation resistance. The results provide a preliminary hypothetical basis for expansion of the applications of soybean protein and the development of fat-soluble active substances for healthy food.

2. Materials and methods

2.1. Materials

LUT (purity > 98%) was acquired from Yuanye Biological Technology Co. (Shanghai, China). SPI (purity > 98%) was obtained from Yuwang Plant Protein Co. (Linyi, China). 8-Anilinonaphthalene-1-sulfonic acid (ANS) was purchased from Sigma–Aldrich Chemical Co. (St. Louis, MO, USA). Sunflower seed oil was acquired from COFCO Fulinmen Food Marketing Co., Ltd. Absolute ethanol and all other chemicals were of analytical grade.

2.2. Formulation of the SPI-LUT nanodelivery system

A certain amount of SPI powder was used to prepare a 0.5 mg/mL solution with 0.01 mol/L PBS buffer, which was stirred at room temperature for 2 h, and then kept for 12 h at 4 °C for complete hydration. The sample was removed and equilibrated at room temperature to obtain the initial SPI solution. By using an ultrasound processor (Scientz-II D, NingBo Scientz Biotechnology Co. Ltd., Ningbo, China) with a 6 mm diameter titanium probe which was dipped into suspension with a depth of 1.5 cm and a distance of 3.0 cm to the bottom, 150 mL of SPI solutions was put into a 250 mL glass vessel which was immersed in an ice-water bath. Then, it was treated under different power outputs for 12 min (5 s: 5 s work/rest cycles) at room temperature to obtain the ultrasonically treated SPI solution [23].

LUT (250 mg) was fully dissolved in absolute ethanol (20 mL) to obtain a luteolin ethanol solution (12.5 mg/mL). LUT solution was added to the original and sonicated SPI solution, stirred at room temperature for 30 min, and then kept from light for 4 h. The mixture was centrifuged at 8000 rpm for 20 min. The resulting supernatant was used for material analysis. The remaining supernatant was frozen at −80 °C for 6 h and then freeze-dried to obtain SPI-LUT powderZhu et al. [62].

2.3. Measurement of the encapsulation efficacy (EE) and loading amount (LA)

The EE and LA were measured by the assay described by Chen et al. [5]. The amount of LUT loaded by SPI was analyzed by extraction spectrophotometry. Two milliliters of complex solution was absorbed into a centrifuge tube, and 20 mL of ethyl acetate solution was added. The mix was evenly mixed with a vortex shaker and maintained at 20 °C away from light. After the solution was layered, the absorption value of the upper liquid at 353 nm was measured by a UV spectrophotometer to calculate the luteolin content. The EE was described as the ratio of LUT in the complexes. The encapsulation efficacy (EE) and loading amount (LA) were calculated as follows.

$$EE(\%) = \left[1 - \frac{content\ of\ free\ LUT(mg)}{total\ content\ of\ LUT(mg)}\right] \times 100$$

$$LA(\mu g/mg) = \frac{total\ LUT\ mass\ (\mu g) - mass\ of\ unbound\ LUT\ (\mu g)}{total\ SPI\ mass\ (mg)}$$

2.4. Solubility measurement

Sample suspensions were prepared at 1% w/v in distilled water. After mixing at room temperature for 1 h, the mixtures were centrifuged at 5000 rpm for 10 min at 20 °C (MR1812 centrifuge, Jouan, Saint-Na-Zaire, France). The supernatant was obtained, and the soluble luteolin content was analyzed by a Bradford test[4]on an ultraviolet–visible spectrophotometer (Lamba 12, Perkin Elmer, San Jose, CA, US) at 353 nm. The solubility was described as follows.

$$S\ (\%) = \frac{LUT\ concentration\ in\ the\ suspension}{initial\ LUT\ concentration} \times 100$$

2.5. Measurement of the particle size and ζ-potential

The particle size was assessed by a dynamic light scattering (DLS) technique, following the method of Morales, Martinez, Pizones Ruiz-Henestrosa, and PilosofMorales et al. [40]. A dynamic Laser Light Scattering instrument (Zetasizer Nano ZS, Malvern Instruments Ltd, Worcestershire, U.K.) was utilized, along with a He–Ne laser (633 nm) and a digital correlator (model MPT-2, Malvern Instruments). The sample prepared as described in section 2.2 was diluted 1000 times and analyzed at 23 °C with a test sample amount of approximately 1 mL.

The ζ-potential of proteins in the SPI and SPI-LUT nanodelivery systems was evaluated by laser Doppler velocimetry and dynamic light scatting techniques using a Malvern Zetasizer Nano ZS instrument (Malvern Instruments Co. Ltd., Worcestershire, UK) at 25 °C.

2.6. Atomic force microscopy (AFM)

A Dimension 3000 microscope (Bruker, Billerica, MA, USA) in tapping mode in air was used to gather atomic force microscopy (AFM) images. The following procedures were used to prepare the samples for AFM measurement: with pH 2.0 Millipore water, SPI-LUT solutions were diluted to a final concentration of 0.5–10 μg/mL. A 2 μL aliquot was placed for 2 min onto freshly sliced mica discs, washed with 1 mL Millipore water, and dried with an air flow. No additional processing was performed once the images were flattened using the Nanoscope Analysis program[41].

2.7. Fluorescence quenching analysis

There are two main mechanisms of fluorescence quenching: static quenching and dynamic quenching[31]. The type of quenching can be determined using the Stern–Volmer equation: $F_0/F = 1 + K_q\,\tau_0\,[Q] = 1$

$+ K_{sv}$ [Q] [47]. Here, F_0 and F represent the fluorescence intensity of the SPI solution without and with the quencher LUT, respectively, [Q] represents the concentration of LUT, K_q is the quenching rate constant of the biological macromolecule, and K_{sv} is the Stern–Volmer quenching constant. The maximum quenching rate constant (K_q) of the various types of fluorescent quenchers for biological macromolecules is on the order of 2.0×10^{10} L·mol^{-1}·s^{-1}. τ_0 is the mean lifetime of the biomolecule fluorophore in the absence of any quencher and is approximately 10^{-8} s [60].

For the static quenching process, the binding constant (K_s), along with the number of binding sites (n), can be calculated via the double logarithmic equation:

$$lg\frac{F_0 - F}{F} = lgK_s + nlg[Q]$$

2.8. Analysis of thermodynamic parameters

The thermodynamic parameters of the SPI-LUT nanodelivery system were measured at 298 K, 306 K and 314 K, including changes in the Gibbs free energy (ΔG), enthalpy (ΔH) and entropy (ΔS). The value of ΔG can be calculated by the following equation: $\Delta G = -RT\ln K_A$ [22]. The ΔH and ΔS can be acquired by the van't Hoff equation: $\ln K_A = -\Delta H/RT + \Delta S/R$, $\Delta G = \Delta H\text{-}T\Delta S$ [36], where T is the absolute temperature, K_A is the binding constant, and R represents the molar gas constant, which is 8.314 J mol^{-1} K^{-1}.

2.9. Fourier transform infrared spectroscopy analysis

The FTIR-ATR spectra of the samples were obtained using a Perkin Elmer FTIR spectrometer (Model System 2000, Perkin Elmer, USA) equipped with a DTGS (deuterated triglycine sulfate) detector and the DuraSampIIR Universal DiComp attachment. Spectra were collected over the range of 400–4000 cm^{-1} at a resolution of 4 cm^{-1}, wavenumber precision of ± 0.01 cm^{-1}, the penetration depth of the KBr crystal ranged from 0.5 to 3.0 mm. For the sample, 32 scans were collected. Perkin Elmer's 9-point block average smoothing technique was used to smooth the spectra once.

2.10. Differential scanning calorimetry (DSC)

A DSC 204F1 thermal analyzer(Netzsch, Germany) was used to test the thermostability of SPI and SPI-LUT nanodelivery system. In an aluminum DSC pan, the complex was combined with PBS buffer (0.01 mol/L, pH 7.2 – 7.4) and equilibrated at room temperature for 12 h. A hermetically sealed aluminum pan holding 10–15 mg of the complex was scanned at a rate of 10 °C/min at a temperature range of 25–150 °C. The pan was quickly cooled to 0 °C after the first scan and reheated under the same heating conditions. Universal Analysis V4.2E was used to calculate several parameters, such as peak denaturation temperature (T_m).

2.11. X-ray diffraction (XRD) analysis

On a Philips PW1730 X-ray diffractometer (PANalytical, Netherlands) equipped with a Cu Kα radiation source, the XRD patterns of samples including pure LUT, SPI, and the SPI-LUT nanodelivery system were recorded in the 2θ range of 5°–60° with an anti-divergence slit of 2/3 and a scan rate of 1π/min. 40 KV and 40 mA were chosen as the operating voltage and filament current, respectively.

2.12. Surface hydrophobicity

Determination of surface hydrophobicity the surface hydrophobicity (H_0) of SPI-polyphenol complexes was determined according to Pessato, Carvalho, Pessato et al. [43], with slight modifications. The anionic fluorescent probe was 1-anilinonaphthalene-8-sulfonic acid (ANS), and 8 mmol/L ANS solution was produced in sodium phosphate buffer (0.1 mol/L, pH 7.4). The samples were diluted in sodium phosphate buffer (0.01 mol/L, pH 7.0) to values of 0.05 to 0.25 mg/mL. Forty microliters of ANS solution was combined with 8 mL of sample diluents and left to react for 8 min in the dark. The fluorescence intensity of the resulting solutions was then measured by a fluorescence spectrophotometer (F-4500, Hitachi, Japan) using buffer with ANS as the blank. The excitation and emission wavelengths were 390 nm and 470 nm, respectively. The plot of fluorescence intensity versus protein concentration was fitted using linear regression. The slope of the curve was used to define the H_0 of the samples.

2.13. Simulated gastric and intestinal digestion

In vitro digestion was performed as a described procedure with some modificationsMinekus et al. [39]. The tested sample (SPI-LUT) was combined with 35 mL of simulated gastric fluid, and 25 mL of NaCl (0.3 mol/L). The pH of the mixture was raised to 2.0 using 0.1 M HCl, and the volume was brought to 92 mL with DI water. Pepsin dispersion (25,000 U/mL, 8 mL) was added, and the mixture was shaken at 95 rpm in a water bath (37 °C). After gastric digestion (1.5 h), The pH was adjusted to 8.0 and the porcine bile salt extract was added. Then, 72 mg trypsin was introduced after 10 min of mixing on a shaking table to begin in vitro digestion of simulated small intestine juice for 2 h. Every 30 min, 10 mL of hydrolysate was removed to simulate the digestive reaction of gastric or intestinal fluids. The response of LUT in buffer without gastric enzymes or pancreatin was used as a blank to eliminate the influence of LUT degradation in the digestion process. The concentration of LUT was measured using HPLC (Waters e2695, Milford, MA, USA) and a UV detector at a wavelength of 353 nm. The bioavailability of LUT can be expressed as the percentage of LUT content in supernatant and the mass of total LUT added before digestion.

2.14. Scavenging activity against DPPH free radicals

The capacity of polyphenols to scavenge DPPH free radicals was measured using a modified version of the approach described by Yen and Wu [57]. Three milliliters of 2×10^{-4} mol/L DPPH free radical solution was combined with three milliliters of sample solution. After 30 min of incubation in the dark, the absorbance of the mixture was measured at 517 nm.

2.15. Statistical analysis

All the data were expressed as means ± standard deviation (SD) of at least three independent measurements. Two-way analysis of variance (ANOVA) was performed for statistical analysis, and the least significant difference (LSD) test with a confidence interval of 95% was utilized to compare the means.

3. Results and discussion

3.1. Evaluation of the encapsulation effect and solubility

3.1.1. Determination of the encapsulation efficacy (EE) and loading amount (LA)

The effects of SPI pretreated with different ultrasonic powers on the encapsulation efficacy and loading amount of LUT are shown in Fig. 1. With the increase in the ultrasonic pretreatment power, the loading amount (LA) of SPI to LUT and encapsulation efficacy (EE) first increased and then decreased. The hydrophobic region in soybean protein is the active region that binds fat-soluble polyphenols. However, due to its spherical structure, the hydrophobic region is wrapped inside, resulting in the low binding rate of natural SPI to LUT. The cavitation impact due to ultrasonic treatment could decrease the intermolecular

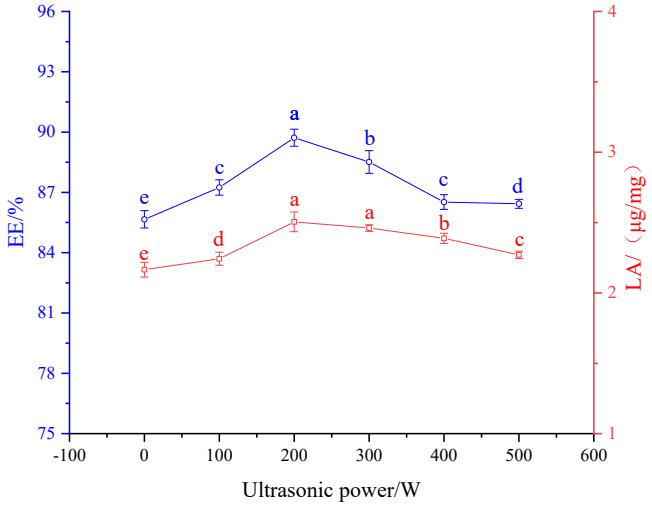

Fig. 1. SPI pretreated with different ultrasonic powers on the Encapsulation efficacy (EE) and loading amount (LA) of LUT.

forces and H-bonds and eventually direct the exposure of earlier veiled hydrophobic groups in the SPI molecules to the exterior circumstances when the protein unfolds[2] (Hao, et al., 2013). Therefore, the adsorption capacity of SPI to LUT is enhanced, resulting in an increase in the EE and LA. When the ultrasonic pretreatment power was 200 W, EE (89.72%) and LA (2.51 μg/mg) reached the highest. The EE and LA decreased with increasing ultrasonic pretreatment power from 200 W to 500 W, signifying that high-power pretreatment of soybean protein isolate will cause protein aggregation reaction and bury hydrophobic regions, resulting in the reduction of binding regions with LUT, which led to the decreases in the LA and EE[7]. Chen et al.[5] found that ultrasonic treatment could extinguish the noncovalent interactions among proteins, including hydrophobic and electrostatic interactions. More hydrophobic sites bound to curcumin were exposed through protein unfolding, resulting in an increase in the LA of the protein to curcumin. This showed that appropriate ultrasonic pretreatment could effectively improve the carrying capacity of SPI for fat-soluble polyphenols.

3.1.2. Solubility measurement

The effect of SPI pretreated with different ultrasonic powers on the solubility of the LUT is shown in Fig. 2. The solubility of LUT was increased approximately 1200 times by complexing with untreated SPI. With the increase in the ultrasonic powers, the solubility of LUT first increased (90.56%) and then decreased. LUT could interact with the hydrophobic region of the protein through hydrophobic interactions and be wrapped by SPI. When the nanodelivery system formed by SPI-LUT contacted the water molecules in the mix, the hydrophilic assemblies of the protein were inserted into the polar environment to improve the water solubility of LUT. ultrasonic pretreatment of SPI was helpful to prolong the protein structure, disconnect the chemical bond between protein peptide chains, and destroy the close relationship between molecules or within molecules. This could promote the structural relaxation and flexibility of protein molecules, enhance the protein-water interaction and protein LUT interaction, and increase the solubility of LUT Ma et al. [35]. With increasing ultrasonic pretreatment power, some unfolded SPI self-aggregates through protein–protein molecular interactions (hydrophobic interactions and S-S bonds) to form dimers, trimers or precipitates, resulting in a decrease in molecular flexibility, which affects the solubility and LUT binding ability and results in a decrease in LUT solubility[61].

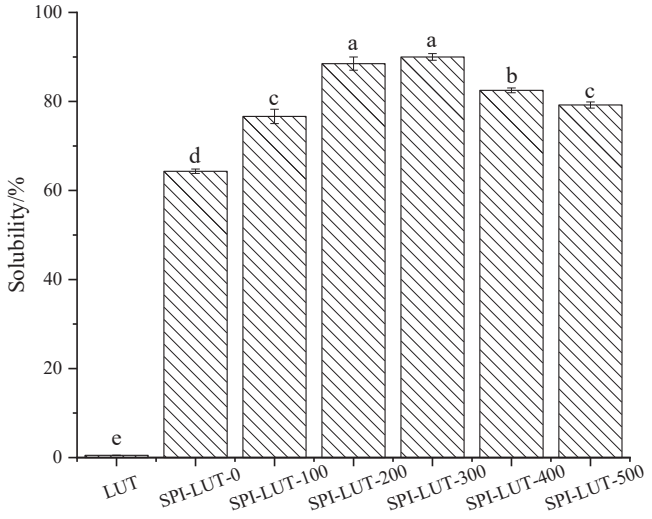

Fig. 2. SPI pretreated with different ultrasonic powers on the solubility of the LUT.

3.2. Morphology analyses

3.2.1. Particle size distribution analysis

Dynamic light diffraction (DLS) technology has become a conventional characterization method in nanotechnology, and can be used to analyze the particle size dispersal and average particle size in the SPI-LUT solution. The particle size distribution curves of untreated SPI and ultrasonic-pretreated SPI-LUT nanodelivery system are shown in Fig. 3. The particle size of the SPI-LUT nanodelivery system was higher than that of SPI, and the monomeric protein peak disappeared. This indicates that LUT particles combine with SPI through certain interactions to form larger particles than SPI monomers. As the ultrasonic pretreatment power was amplified from 0 to 200 W, the particle size of the SPI-LUT nanodelivery system decreased gradually, the particle size distribution diagram changed from a high and narrow peak to a low and wide peak, and there were double peaks in the particle size delivery of the nanodelivery system. With low-power ultrasound treatment, the impacts of turbulent forces and microstreaming might increase the rapidity of protein smashing and dissociation, leading to an increase in hydrophobicity and the formation of smaller soluble protein aggregatesTomé Constantino and Garcia-Rojas [9,27]. This process was demonstrated to be very effective in encapsulating hydrophobic bioactive compounds in the reassembled SPI micelles [5]. The small particle size SPI-LUT nanodelivery system had a larger adsorption superficial

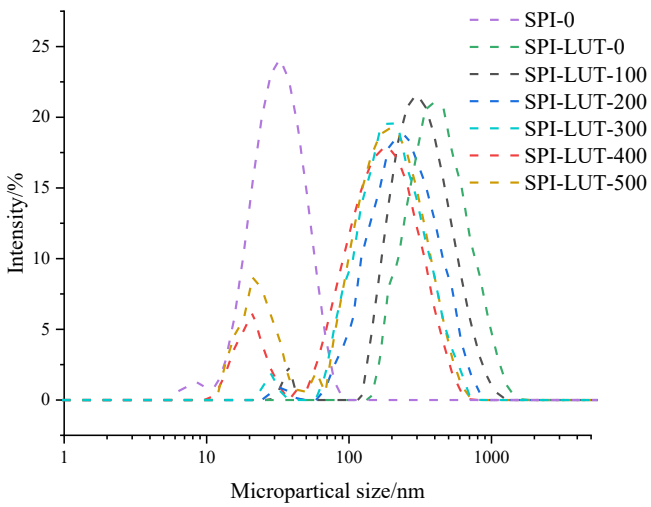

Fig. 3. Particle size distribution of the untreated SPI and ultrasonically pretreated SPI-LUT nanodelivery system.

extent, which enhanced the binding affinity between SPI and LUT and was more conducive to the improvement of LUT solubility and bioavailability. When the ultrasonic pretreatment power surpassed 300 W, the peak position with a particle size distribution of 10–100 nm was consistent with the particle size distribution of SPI alone, indicating that when the ultrasonic pretreatment power surpassed 300 W, the content of SPI that was not combined with LUT in the solution increased. Therefore, the protein structure of SPI under high-power treatment was not suitable for combination with LUT. The high ultrasonic pretreatment power might also initiate fractional denaturation and microstructural changes (e.g., occurrence of aggregation or dissociation and/or reassociation) of proteins, which might increase the degree of aggregation and decrease the hydrophobicity to protect the hydrophobic regions of the proteins (Li et al., 2020), [18]. These structural changes were detrimental for the embedding of LUT into the proteins.

3.2.2. ζ-potential testing

The ζ-potential was conceptualized to indicate strength on the surface of particles and reflect the intensity of electrostatic repulsion or attraction [52]. Consequently, the ζ-potential dimension is a significant index to measure the steadiness of the complex in solution. The ζ-potential profiles of the untreated SPI and ultrasonically pretreated SPI-LUT nanodelivery system are shown in Fig. 4. The potential of the untreated SPI solution was -14.93 ± 0.14 mV, when LUT was added, the absolute value of ζ-potential increased significantly. It was apparent that the introduction of LUT changed the distribution of charged groups at the surface of the SPI, which was possibly explained by the neuralization of the positively charged groups of protein by the negatively charged polyphenols. Sui et al. [49] also described that the total ζ-potential of soybean protein increased after combination with anthocyanin. With the increase of ultrasonic pretreatment power, the absolute ζ-potential of the nanodelivery system changed irregularly. When the ultrasonic pretreatment power was 200 and 400 W, the ζ-potential reached the maximum. This indicates that appropriate ultrasonic pretreatment of SPI was helpful to increase the absolute ζ-potential of the nanodelivery system for better solution stability. This might be because appropriate ultrasonic pretreatment power is conducive to the binding of SPI and LUT, further changing the protein structure, resulting in an increase in surface charges and a decrease in particle size of SPI-LUT nanodelivery system. Commonly speaking, a level >20 mV indicates that the solution system is steadier. When the ultrasonic pretreatment power was 200 and 400 W, the absolute ζ-potential of the SPI-LUT nanodelivery system exceeded 40 mV, which indicated that a more stable solution system is formed. Zhao et al. (2017) showed that ultrasonic treatment caused the exposure of charged groups in red bean protein, resulting in higher absolute value of ζ-potential potential of red bean protein-lutein complexes. This indicated that appropriate ultrasonic pretreatment power changed the structure of SPI and formed a more stable SPI-LUT nanodelivery system.

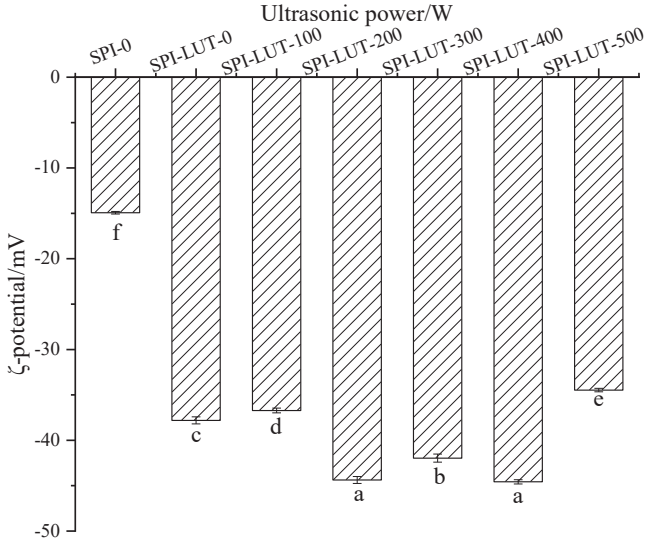

Fig. 4. ζ-potential of the untreated SPI and ultrasonically pretreated SPI-LUT nanodelivery system.

3.2.3. AFM

AFM offers nanoscale data on aggregate generation in solid samples and has been utilized to determine the morphology of protein-phenolic campuses. To further understand the alterations in the nanoscale structure of untreated SPI and ultrasonically pretreated SPI-LUT nanodelivery system, AFM analyses were conducted for native samples and samples after ultrasonic pretreatment, and the results are shown in Fig. 5. The nontreated SPI showed a regular and dissociated morphology. When LUT was loaded, it could be observed that the particle diameter increased as well as the density. The results show that the nanodelivery system was formed, and the micromorphology of the nanoparticles was related to the loading amount of LUT [45]. When the ultrasonic pretreatment power was 200 W and 300 W, the SPI-LUT nanodelivery system with a smaller particle size was more uniformly dispersed, which might contribute to the solubility and stability of the nanodelivery system and the stable release state when simulating in vitro digestion [13]. However, when the ultrasonic power was too high, cluster particles with larger particle sizes appeared in the SPI-LUT nanodelivery system, and the distribution was dense. This was due to the strong cavitation caused by excessive ultrasonic treatment, which destroyed the interaction between protein molecules, made the protein refold to form large particles, and affected the micromorphology and dissolution characteristics of the SPI-LUT nanodelivery system [15].

3.3. Structural analyses

3.3.1. Intrinsic fluorescence analysis

Intrinsic fluorescence is an effective method to study the interactions of proteins with polyphenols Zhang et al. [59]. When excited at 280 nm, the protein intrinsic fluorescence near 340 nm is mainly induced by the emission of tyrosine (Tyr) and tryptophan (Trp), and reductions in the fluorescence intensities indicate interactions between proteins and quenching molecules via ligand binding [58]. The fluorescence spectra of untreated and ultrasonically pretreated SPI following the addition of 0–100 mM LUT at 298 K, 306 K, and 314 K are shown in Fig. 6. The fluorescence strength of SPI declined progressively, and the peaks showed a minored change with increasing concentration of LUT. Preceding investigators have noted that the fluorescence strength of proteins such as zein and gluten was also reduced when the concentration of added resveratrol was increased, due to binding between polyphenols and proteins [29]. In addition, the results indicate that the skeleton of the protein became loosened and unfolded under the interaction between SPI and LUT, and the hydrophobicity of the microenvironment of SPI was reduced. Different degrees of redshifts in the maximal emission wavelengths of the unheated and ultrasonically pretreated SPI-LUT nanodelivery systems were observed, which indicate that the realignment of Trp and Tyr residues in the protein microenvironment may have changed their protein secondary structure because of their binding interactions with LUT. Additionally, the change in the magnitude of the binding affinity with ultrasonic power could be attributed to the aggregation of protein monomers under different ultrasonic power conditions. Fig. 7 shows that the quenching efficacy of LUT on native and ultrasonically pretreated SPI fluorescence varied under different ultrasonic pretreatment powers, and the values of K_{sv} and K_q are summarized in Table 1, indicating the occurrence of LUT-induced protein fluorescence quenching, which followed the Stern–Volmer equation. The Stern-Volmer plots presented a decent linear association at three dissimilar temperatures (Fig. 7) ($R^2 > 0.99$), signifying that the quenching was

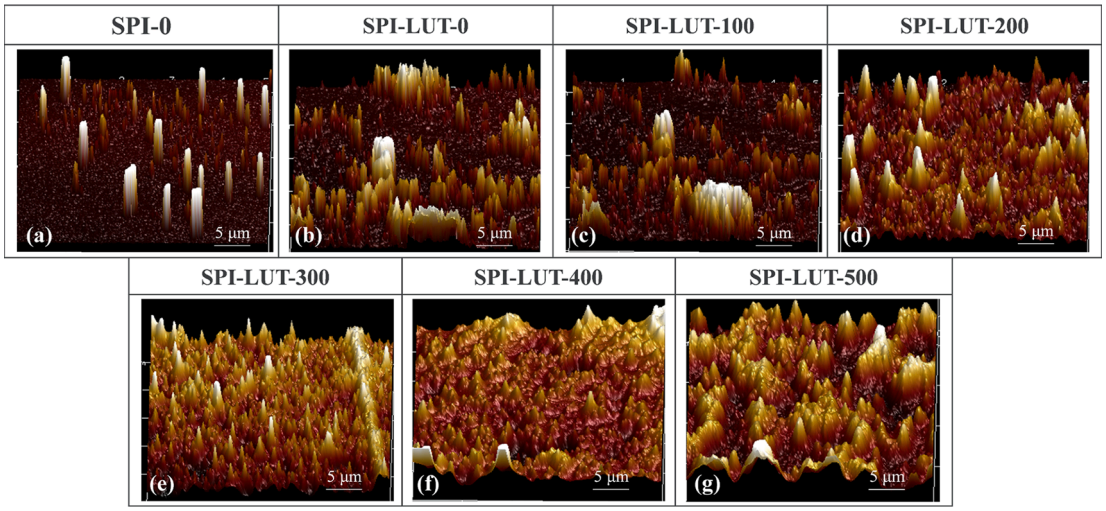

Fig. 5. Atomic force microscopy of untreated SPI and ultrasonically pretreated SPI-LUT nanodelivery system.

produced by static means. As revealed in Table 1, the level of K_{sv} of the SPI-LUT nanodelivery system decreased with increasing temperature. At the same temperature, with the increase in ultrasonic power, the K_{sv} of the nanodelivery system first decreased and then increased, which indicates that the quenching effect of the nanodelivery system was affected by protein of ultrasonic pretreatment. The minimum biomolecular quenching rate constant K_q of the compounds was 1.00×10^{12} $L{\cdot}mol^{-1}{\cdot}s^{-1}$, which was greater than the maximum diffusion collision quenching constant (2×10^{10} $L{\cdot}mol^{-1}{\cdot}s^{-1}$). This further shows that the quenching process of LUT on SPI was due to the static quenching caused by molecular binding compounds, which was consistent with previous studies [11].

3.3.2. Analysis of quenching type and binding degree

Fig. 8 shows the double logarithm regression plots of $lg\frac{F_0-F}{F}$ against lg [Q]. The values of n and K_s expressed based on the slopes of the individual plots are also tabulated in Table 1. The values obtained for n were affected by the ultrasonic pretreatment power and ranged from 0.62 to 2.01, indicating that one or two LUT molecules were bound to one protein molecule. When the ultrasonic pretreatment power was between 100 W and 300 W, the values obtained for n were close to 2 at 298 K. However, the n values decreased with increasing ultrasonic pretreatment power force from 300 W to 500 W, signifying that a suitable ultrasonic pretreatment power could improve the binding site in SPI for LUT during the interaction due to the open protein structure [33]. Treatments that open the protein structure, such as heat treatment, pH treatment, high-pressure treatment, and alcohol-mediated treatment, can also increase the interaction spots between polyphenols and proteins [37]. In the fixed ultrasonic pretreatment power condition, the binding constant K_s of SPI decreased with increasing temperature, signifying that the reaction is exothermal. The binding constant K_s of SPI at the same temperature first increased and then decreased with increasing ultrasonic pretreatment power, indicating that ultrasonic pretreatment directly increased the affinity between SPI and LUT. The enhanced interaction capability could be attributed to the increased unfolding protein and surface hydrophobicity, which could expose more hydrophobic groups and enhance hydrophobic interactions between minor molecules and proteins [16].

3.3.3. Analysis of the thermodynamic parameters

The thermodynamic parameters related to SPI-LUT binding could be calculated from the given findings. The findings in Table 2 display that all $\Delta G < 0$ at dissimilar temperatures, signifying that the binding between SPI and LUT was spontaneous reactions driven by Gibbs free energy [22]. Four kinds of key noncovalent binding powers are involved in the interaction between proteins and small molecules, including H-bonding, electrostatic interactions, van der Waals forces, and hydrophobic interactions. If $\Delta H < 0$ and $\Delta S > 0$, electrostatic interactions are the key forces; if $\Delta H > 0$ and $\Delta S > 0$, hydrophobic action plays the main role; if $\Delta H < 0$ and $\Delta S < 0$, the key forces are hydrogen bonds and van der Waals forces [53]. Therefore, the interaction of SPI with LUT is mainly determined by hydrophobic forces. The study findings are similar to those of previous studies, which showed that resveratrol and gliadin are mainly bonded by hydrophobic interactions. [29].

3.3.4. Fourier transform infrared spectroscopy analysis

FTIR spectroscopy is an established assay to describe the secondary structure of proteins. To examine the matter of an exact kind of secondary protein structure influenced by SPI-LUT interactions, FTIR spectroscopy was performed (Fig. 9). The C–O stretching vibrations of the peptide backbone in the amide I band (1600–1700 cm^{-1}) can provide information about several secondary structures (α-helix, β-sheet, etc.) [26]. Specifically, bands at 1610–1640 cm^{-1}, 1640–1650 cm^{-1}, 1650–1660 cm^{-1} and 1660–1695 cm^{-1} are allocated to β-sheet, random coil, α-helix and β-turn structures, respectively. Table 3 provides the calculated percentage of protein secondary structures for the SPI-LUT nanodelivery system. There was no new characteristic peak in the infrared spectrum during the nanodelivery system complexation, implying that the formation of the SPI-LUT nanodelivery system was only the transfer of chemical bonds, and no new chemical bonds were formed. Amide I (1700–1600 cm^{-1}) and amide II (1600–1500 cm^{-1}) bands mostly signify C–O stretching and N–H bending of amide bonds, respectively. The peaks of the amide I and II bands for SPI-LUT-0 were 1592.3 and 1646.4 cm^{-1}, respectively, and 1600.2 and 1650.7.cm^{-1} for SPI-LUT-100, respectively. However, the peaks of the amide I and II bands for SPI-LUT-200 shifted to 1613.2 and 1660.4 cm^{-1}, respectively, and with increasing ultrasonic prepower, amide I and amide II were still changing. These alterations in the amide I and II bands show that intermolecular electrostatic forces occurred between SPI and LUT, but the shift was insignificant, suggesting that electrostatic interaction occurred but was not the key force. Additionally, LUT is a hydrophobic compound, and SPI also has some hydrophobic groups; thus, hydrophobic impacts might also be an interaction force. This is also indicated by the analysis of thermodynamic parameters. The combination of the two is mainly hydrophobic interaction but is accompanied by electrostatic force. Similarly, Dai et al. [10] utilized FTIR spectroscopy to explain the presence of electrostatic forces.

Table 3 shows the composition of unmodified SPI: 23.04% α-helix, 36.82% β-sheet, 10.85% β-turn, and 29.29% random coil. Compared

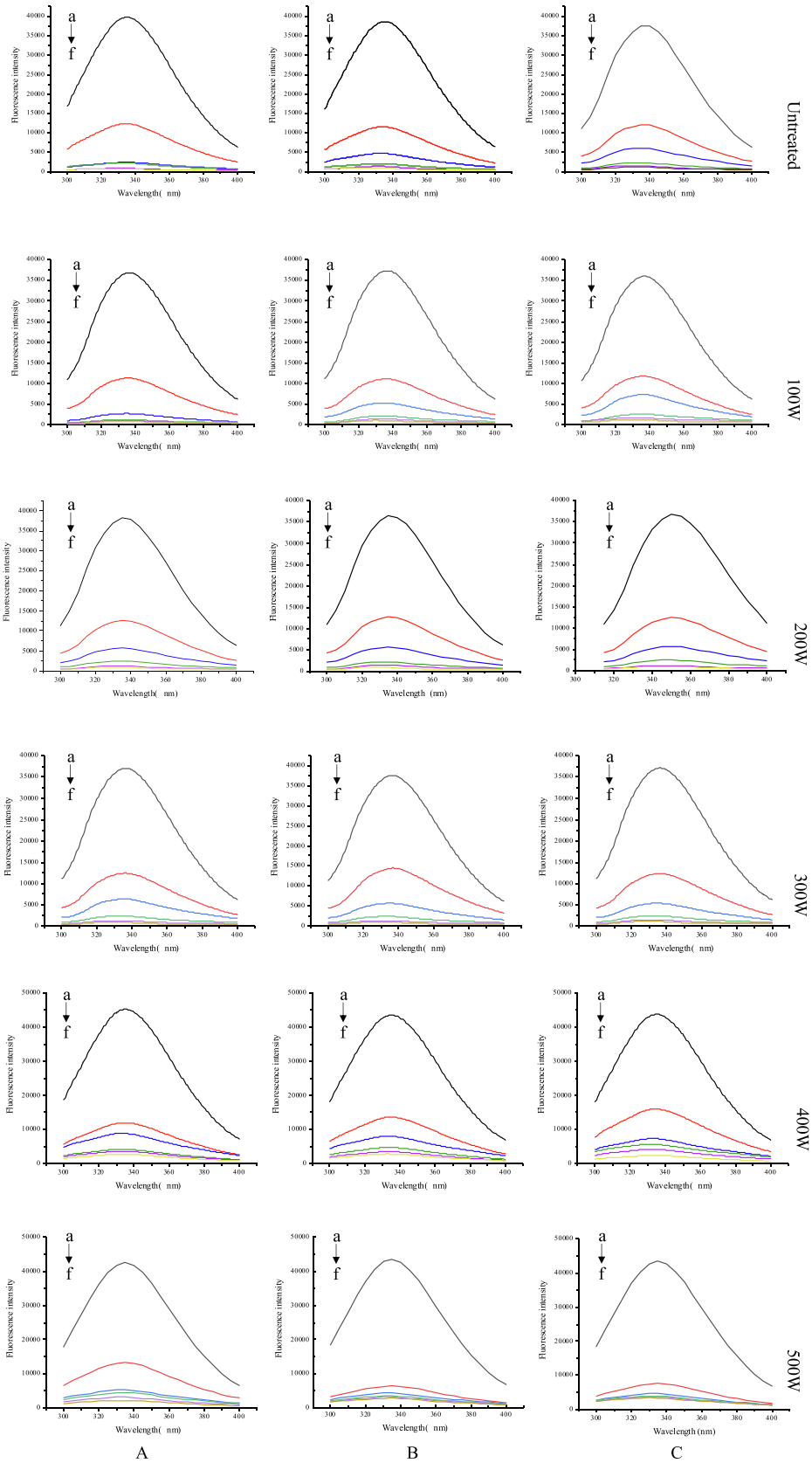

Fig. 6. Effect of LUT on the fluorescence spectrum of ultrasound-treated SPI.

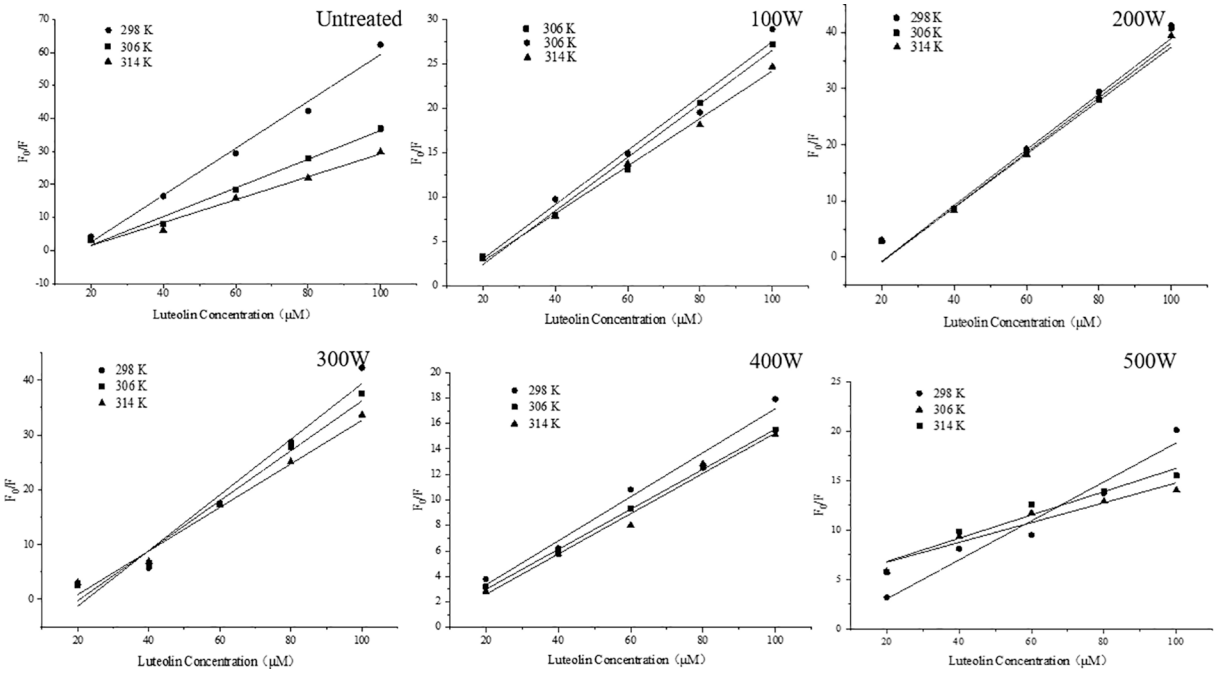

Fig. 7. Stern-Volmer plots for fluorescence quenching at different temperatures.

Table 1
Fluorescence quenching constants, bimolecular quenching rate constant, apparent binding constants, binding site numbers and correlation coefficients of SPI-LUT nanodelivery system at different temperatures.

Sample	Temperature/K	K_{sv} ($\times 10^4$ L·mol^{-1}·s^{-1})	K_q ($\times 10^{12}$ L·mol^{-1}·s^{-1})	R_1^2	K_s/M	n	R_2^2
SPI-LUT-0	298	7.1045	7.1045	0.9851	109.4460	1.6535	0.9714
	306	4.3422	4.3422	0.9860	26.7454	1.4701	0.9707
	314	3.4744	3.4744	0.9761	21.4981	1.3919	0.9960
SPI-LUT-100	298	3.0691	3.0691	0.9791	5943.1953	2.0098	0.9919
	306	3.0159	3.0159	0.9955	502.2501	1.7820	0.9961
	314	2.6792	2.6792	0.9957	840.1201	1.6129	0.9849
SPI-LUT-200	298	4.9595	4.9595	0.9472	1501.2741	1.8853	0.9962
	306	4.8809	4.8809	0.9403	1989.7016	2.0169	0.9957
	314	4.7629	4.7629	0.9437	1411.6924	1.9632	0.9965
SPI-LUT-300	298	5.0767	5.0767	0.9397	3002.6865	1.8874	0.9693
	306	4.5576	4.5576	0.9649	4288.9442	2.0080	0.9910
	314	3.9747	3.9747	0.9756	515.8816	1.7924	0.9881
SPI-LUT-400	298	1.7279	1.7279	0.9699	470.8954	1.1126	0.9820
	306	1.5698	1.5698	0.9977	863.6455	1.1914	0.9983
	314	1.5804	1.5804	0.9805	1910.3669	1.2791	0.9913
SPI-LUT-500	298	1.9711	1.9711	0.9479	2117.7329	1.2664	0.9619
	306	1.1178	1.1178	0.9277	890.3204	0.6906	0.9688
	314	1.0019	1.0019	0.9162	430.2395	0.6240	0.9700

with SPI, the β-sheet and random coil content of the SPI-LUT nanodelivery system decreased, and the α-helix content increased. There was also a correlation between the rise in α-helix and the decline in β-sheet and random coil [55]. These outcomes suggest that the noncovalent binding of LUT to SPI promoted the conversion of β-sheet regions and random coil regions to α-helix regions, and the increase in α-helix content also indicates that the interior of the protein shrinks with the addition of LUT. In addition, with the increase of ultrasonic pretreatment power from 0 W to 500 W, the SPI-LUT nanodelivery system α-helix, β-sheet and β-turn all decreased first and then increased, while the random coil content changed irregularly, but the ultrasonic pretreatment power of each secondary structure content reaching the peak was different. When the ultrasonic pretreatment power was 200 W, the SPI-LUT nanodelivery system α-helix content was the lowest. This shows that the structure of SPI-LUT-200 W is looser and more stretched, and the hydrophobic and polar groups inside proteins are exposed to the surface. This structure helps to increase the interaction between the SPI and LUT and causes the SPI to load the most LUT at this power. LUT was inserted into the hydrophobic surface of SPI and destroyed its hydrogen bond network, leading to a decrease in α-helix [49]. Dai et al. [11] considered the changes in secondary structure after the combination of protein and polyphenols in the interaction between rice protein and resveratrol, and the content of the α-helix (to 7.8%) and β-sheet (to 22.1%) regions decreased, while the content of the β-turn (to 35.9%) and random coil (to 34.1%) regions were amplified. However, the secondary structure change of the nanodelivery system was not completely regular. Zhao et al. [61] researched that ultrasound treatment can affect the α-helix and β-sheet structure by breaking hydrogen bonds. Hao et al. [20] found that the addition of polyphenols could lead to the reorganization of the secondary structure of protein. Therefore, the secondary structure of SPI-LUT nanodelivery system is jointly affected by ultrasonic treatment and polyphenols, resulting in irregular alterations in the secondary structure of the nanodelivery system.

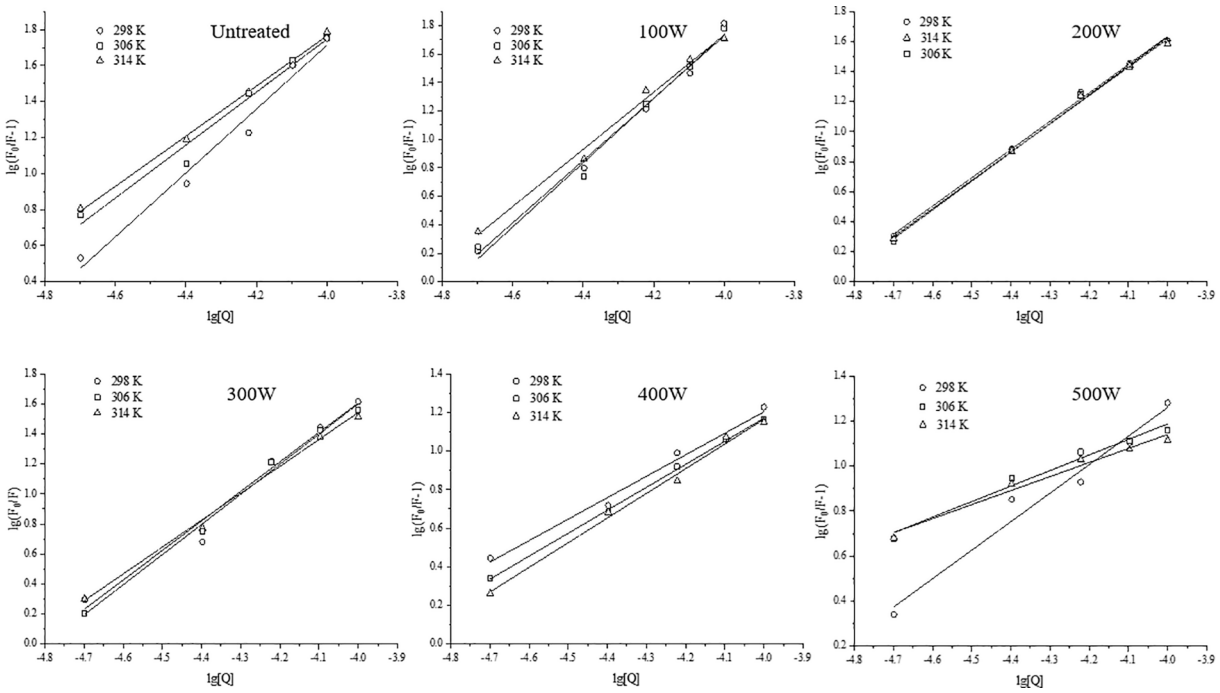

Fig. 8. Double logarithm diagram of SPI with different ultrasonic pretreatments was quenched LUT at different temperatures.

Table 2
Thermodynamic binding parameters for SPI-LUT nanodelivery system at different temperatures.

Sample	Temperature/K	△H/(KJ/mol)	△S(J/mol·K)	△G(KJ/mol)
SPI-LUT-0	298	133.54	0.49	−11.63
	306		0.46	−8.36
	314		0.45	−8.01
SPI-LUT-100	298	234.17	0.86	−21.53
	306		0.82	−15.82
	314		0.80	−17.58
SPI-LUT-200	298	234.27	0.18	−18.12
	306		0.18	−19.33
	314		0.17	−18.93
SPI-LUT-300	298	211.50	0.78	−19.84
	306		0.76	−21.28
	314		0.73	−16.31
SPI-LUT-400	298	179.72	0.32	−15.25
	306		0.32	−17.20
	314		0.32	−19.72
SPI-LUT-500	298	182.12	0.34	−18.97
	306		0.32	−17.28
	314		0.31	−15.83

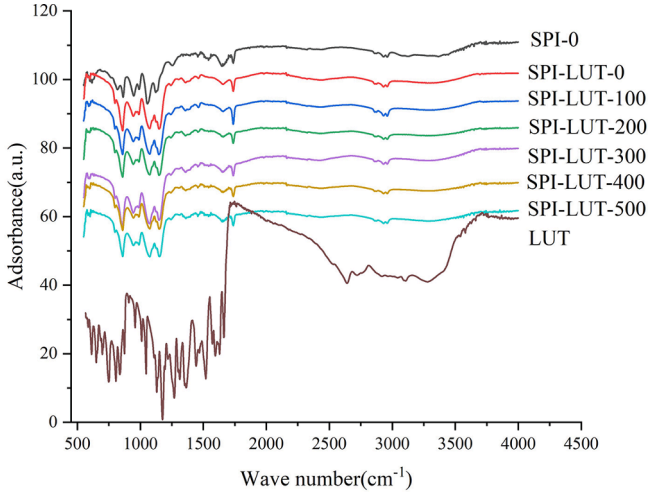

Fig. 9. FTIR spectra of LUT, SPI and the ultrasonically pretreated SPI-LUT nanodelivery system.

3.3.5. *Differential scanning calorimetry (DSC)*

DSC has the advantage of being a widespread assay to analyze protein thermal denaturation and thermodynamics. To analyze the thermal stability of the SPI-LUT nanodelivery system, DSC analysis was performed (Fig. 10). T_m reflects the temperature at which denaturation of the nanodelivery system occurred (Table 4). The SPI thermal denaturation curve presents a concave shape, showing an exothermic effect, and T_m was 96.03 ± 1.22 °C. While the peak area of the thermal denaturation curve increased after SPI and LUT formed the nanodelivery system, the peak type did not change significantly, and the T_m value increased. LUT had high crystallinity, and its melting point could reach 350 °C, where there will be an endothermic peak [25] However, no melting peak of LUT was recorded in the SPI-LUT nanodelivery system, indicating that LUT was embedded. The increase in the T_m value of the nanodelivery system may be due to the noncovalent binding of SPI and LUT. Liu et al. [34] demonstrated that the adjustment of proteins by quinines increased their thermal denaturation temperatures. Meng et al. [38] found that the ferritin shell may protect encapsulated polyphenols by forming hydrogen bonds, hydrophobic forces and van der Waals interactions between polyphenols and ferritin, which can improve the stability of the nanodelivery system. Other reports have also revealed that the combination of polyphenols and protein could increase the thermal constancy of the nanodelivery system, which was linked to the binding between proteins and polyphenols [34]. In addition, the enhancement of thermal stability was closely related to the ultrasonic pretreatment power. With the increase of ultrasonic pretreatment power, the peak tip of the thermal denaturation curve of the SPI-LUT nanodelivery system continued to move to the right, and T_m continued to increase. When the ultrasonic pretreatment power exceeded 300 W, although T_m increased slightly, the change was not significant. ultrasonic pretreatment can cause the incomplete or whole unfolding of proteins; this might additionally produce the re-aggregation of protein. The aggregation step includes

Table 3
Percentages of protein secondary structures in the SPI-LUT nanodelivery system.

Sample	α-helix/%	β-sheet/%	β-turn/%	Random coil/%
SPI-0	23.04 ± 0.32^{d}	36.82 ± 0.26^{a}	10.85 ± 0.12^{d}	29.29 ± 0.16^{a}
SPI-LUT-0	26.80 ± 0.36^{b}	30.92 ± 0.21^{b}	16.53 ± 0.14^{a}	25.75 ± 0.11^{b}
SPI-LUT-100	27.25 ± 0.63^{b}	27.76 ± 0.12^{c}	16.00 ± 0.17^{c}	24.98 ± 0.11^{c}
SPI-LUT-200	21.16 ± 0.37^{c}	27.00 ± 0.19^{c}	19.61 ± 0.09^{b}	22.23 ± 0.12^{d}
SPI-LUT-300	23.58 ± 0.34^{d}	26.23 ± 0.29^{d}	25.73 ± 0.15^{a}	24.46 ± 0.08^{c}
SPI-LUT-400	23.21 ± 0.19^{d}	26.10 ± 0.24^{d}	25.63 ± 0.18^{a}	24.07 ± 0.15^{c}
SPI-LUT-500	29.59 ± 0.18^{a}	27.46 ± 0.14^{b}	26.52 ± 0.24^{a}	16.42 ± 0.26^{e}

Note: Comparisons were carried out between values of the same column; values with a different letter(s) indicate a significant difference at $p \leq 0.05$.

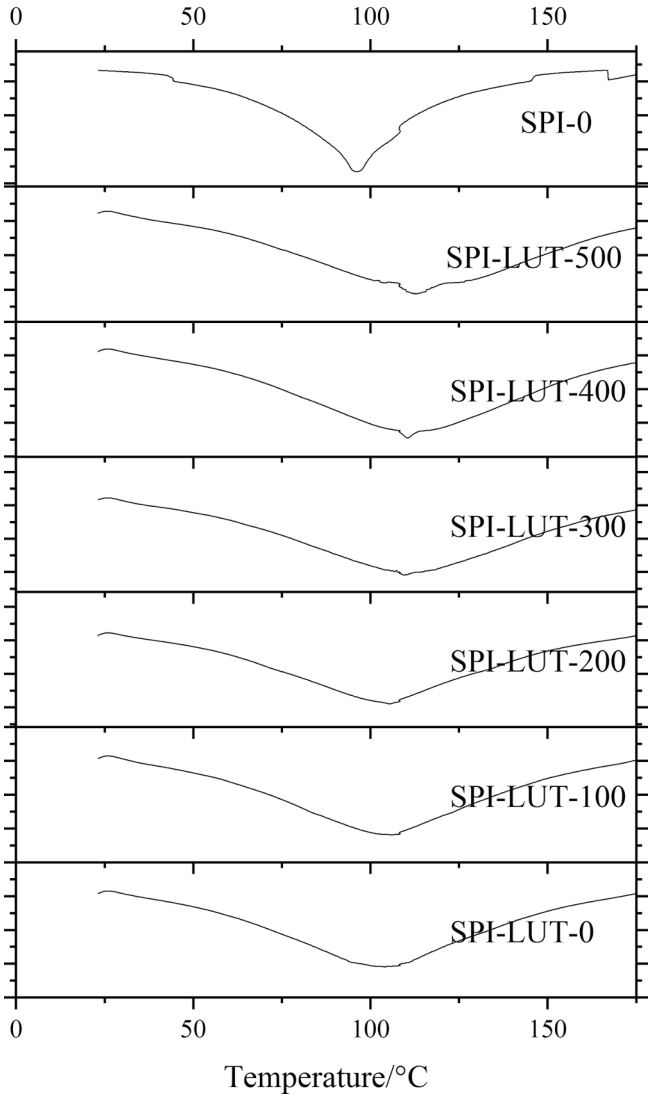

Fig. 10. Effects of ultrasonic treatment on the thermal stability of the SPI-LUT nanodelivery system.

forming novel inter- or intramolecular bonds in the protein particles [24]. This alteration is estimated to modify the protein thermal stability and modify the thermal steadiness of the nanodelivery system, therefore offering a different DSC endotherm.

Table 4
Influence of ultrasonic pretreatment on the thermal denaturation temperature of the SPI-LUT nanodelivery system.

Sample	T_m/°C
SPI-0	96.03 ± 1.22^{d}
SPI-LUT-0	103.34 ± 0.86^{c}
SPI-LUT-100	105.89 ± 0.79^{b}
SPI-LUT-200	105.52 ± 1.80^{b}
SPI-LUT-300	109.55 ± 1.47^{a}
SPI-LUT-400	110.46 ± 1.03^{a}
SPI-LUT-500	112.66 ± 1.69^{a}

Note: Comparisons were carried out between values of the same column; values with a different letter(s) indicate a significant difference at $p \leq 0.05$.

3.3.6. X-ray diffraction (XRD) analysis

XRD analysis was employed to examine the structural phase of dissimilar samples. As illustrated in Fig. 11, LUT possesses a series of crystalline peaks at $2\theta = 21.00$, 23.32, 25.44, and 28.88°, corresponding to its highly crystalline structure [32]. On the other hand, the diffraction pattern of native SPI exhibits two distinguishable peaks at $2\theta = 31.67$ and 45.41°, suggesting a partially crystalline structure. When SPI and LUT formed a nanodelivery system, the XRD pattern was similar to that of pure SPI, and the diffraction peaks of LUT were smeared. This result indicates that LUT particles were effectively embedded into the matrix formed by SPI and formed amorphous LUT. Moreover, with the increase of ultrasonic pretreatment power, the diffraction angle was 2θ between 30.0–35.0 and 45.0–55.0, and the height of the diffraction peak of SPI-LUT nanodelivery system first increased and then decreased. The height variation of the diffraction peak of SPI-LUT nanodelivery system represents the different number of amorphous structures formed [61]. Wan et al. [51] showed that embedding crystalline materials into the nanodelivery system is conducive to the increase of amorphous structure of the system, this will increase the solubility of crystalline substances. Therefore, we speculate that under the 200 W power ultrasonic pretreatment, the diffraction peak intensity of SPI-LUT nanodelivery system is the highest, indicating that more amorphous structures are formed. This may be the reason for the highest solubility of SPI-LUT-200 nanodelivery system.

3.3.7. Determination of surface hydrophobicity

ANS was exploited as a fluorescent probe to detect hydrophobic sites and explore the conformational changes in the SPI-LUT nanodelivery system. As shown in Fig. 12, a significant ($p < 0.05$) decrease in surface

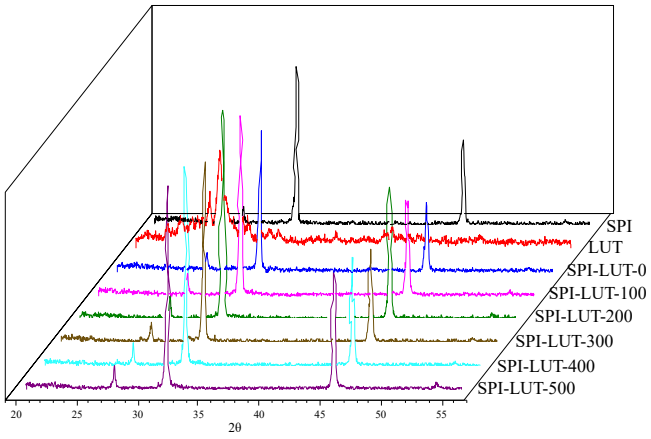

Fig. 11. X-ray diffraction of the ultrasonically pretreated SPI-LUT nanodelivery system.

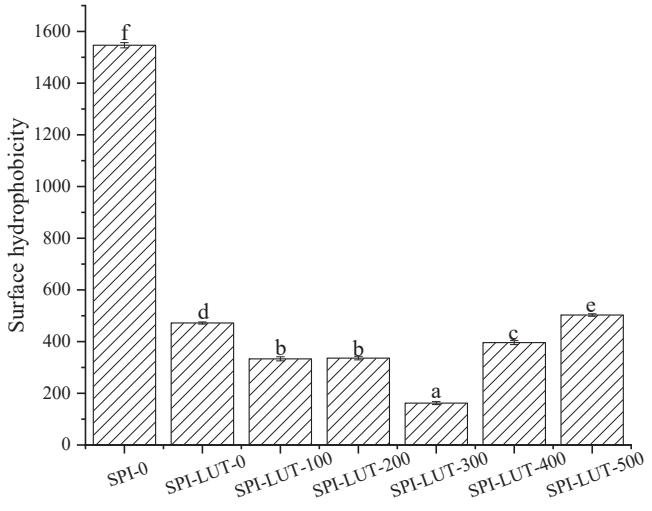

Fig. 12. Effects of ultrasonic pretreatment on the surface hydrophobicity of the SPI-LUT nanodelivery system.

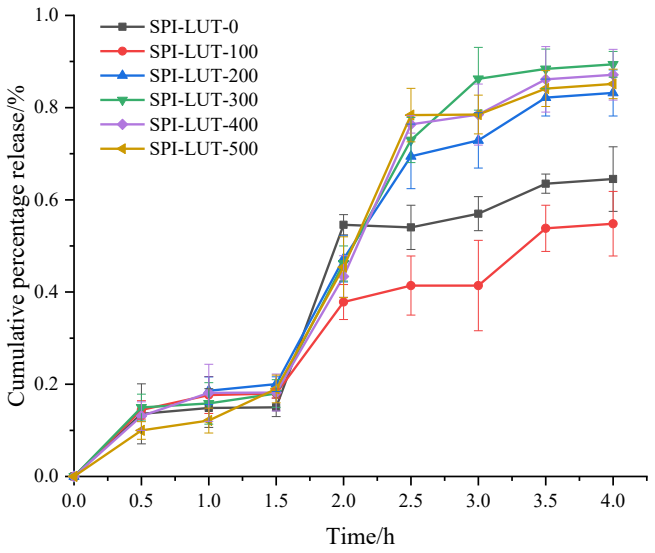

Fig. 13. LUT release rate of the SPI-LUT nanodelivery system with different ultrasonic pretreatments in gastrointestinal digestion.

hydrophobicity was noted in the SPI-LUT nanodelivery system after binding with LUT. This might be because the SPI-LUT nanodelivery system was shaped via hydrophobic binding. When SPI binds with LUT, it undergoes conformational alterations and structural opening. At the same time, LUT is embedded into the hydrophobic region of the protein through hydrophobic interactions, which will bury some hydrophobic groups of the protein and introduce the hydrophilic group (hydroxyl) of LUT itself, resulting in a decrease in the surface hydrophobicity of the SPI-LUT nanodelivery system. The aggregation of proteins induced by the addition of polyphenols may be another motive for the reduction in the surface hydrophobicity of the SPI-LUT nanodelivery system. With the improvement in ultrasonic power, the surface hydrophobicity of the SPI-LUT nanodelivery system first decreased and then increased, and the surface hydrophobicity of SPI-LUT-300 was the lowest. The hydrophobic region of natural SPI is buried inside the molecule, and the appropriate ultrasonic-induced cavitation phenomenon will expose some hydrophobic regions of SPI to the molecular surface, which is conducive to noncovalent binding between phenols and proteins under hydrophobic interactions, resulting in the lower hydrophobicity of the SPI-LUT nanodelivery system. When the ultrasonic pretreatment power continues to increase, the surface hydrophobicity of the nanodelivery system is enhanced. Under high-power pretreatment, ultrasound can also change the tertiary structure of SPI, leading to the unfolding of protein and the extension of noncovalent bonds of protein molecules and increasing the number of hydrophobic groups and regions in molecules exposed to a polar environment. However, this will also lead to a decrease in protein flexibility and an increase in protein aggregation [42]. The SPI-bound LUT is reduced, thereby reducing the effect of LUT on the hydrophobic groups on the surface of the nanodelivery system. Under high-power pretreatment, the increase in H_0 by ultrasound outweighed the reduction in H_0 by the binding of LUT, which increased the surface hydrophobicity of the SPI-LUT nanodelivery system. This is consistent with the LA and EE results for the nanodelivery system.

3.4. Analysis of bioavailability

3.4.1. Simulated gastric and intestinal digestion

Bioavailability was determined by the concentration of LUT released by gastrointestinal digestion in vitro [8]. The release rate of LUT during gastrointestinal digestion is shown in Fig. 13. With the extension of digestion time, the release of LUT in SPI-LUT increased gradually, and the release of LUT in SIF was higher than that in SGF. During the first 1.5 h of gastric digestion, the release rate of LUT in the untreated and ultrasound-pretreated SPI-LUT nanodelivery systems was <20%, and there was no significant difference between the untreated and ultrasound-pretreated SPI-LUT nanodelivery systems at the end of gastric digestion (1.5 h). This showed that after the combination of LUT and SPI, the protective effect of SPI inhibited the activity of oxidase in the gastrointestinal tract so that LUT could be smoothly transported to the small intestine through the upper gastrointestinal tract, thus reducing the release of LUT in the stomach. Then, in SIF, the LUT release rate of the ultrasound-pretreated SPI-LUT nanodelivery system was higher than that of SPI-LUT-0. At the end of intestinal digestion (2.5 h), the LUT release rate of SPI-LUT-0 was 64.51%, and the highest release rate of 200–400 W samples treated with ultrasound was 89.40%. Therefore, ultrasonic pretreatment of the SPI-LUT nanodelivery system inhibited the release of LUT in SGF but promoted its release in SIF. The release rate of LUT under different ultrasonic pretreatment powers varies. This may be because appropriate ultrasonic pretreatment power can open the protein structure and improve the flexibility of protein molecules to expose more trypsin recognition sites [56]. Xue et al. [54] showed that polyphenols can increase the α-helix content of protein secondary structure, and more protease target sites were exposed in protein, thereby promoting the enzymatic reaction of proteases. Therefore, the changes of protein conformation induced by ultrasound and polyphenols are helpful to trypsin hydrolyze SPI-LUT nanodelivery system and improve the release rate of LUT. However, high-power ultrasonic pretreatment will lead to protein aggregation and the formation of tight and orderly structures, resulting in a reduction in protein digestibility [17]. This is not conducive to the enzymatic hydrolysis of the SPI-LUT nanodelivery system by trypsin in the intestine. Therefore, the pretreatment of SPI with appropriate power can better protect LUT from the degradation caused by gastric acid corrosion and promote its large release in SIF to promote the bioavailability of LUT.

3.4.2. DPPH free radical scavenging effect

The antioxidant effect of phenolic compounds versus DPPH free radicals could be assessed by their capability to relieve electrons or H-atoms Achat et al. [1]. As shown in Fig. 14, the DPPH elimination rate of samples without in vitro simulated digestion was low, and the DPPH elimination ratio of all samples was no >15%, which indicates that LUT was encapsulated by SPI. Under high encapsulation efficiency, LUT could not release hydrogen or electrons, resulting in a low DPPH elimination rate of the samples. After simulated gastric digestion in vitro, the DPPH clearance of all samples increased significantly, and with the increase of ultrasonic pretreatment power, the DPPH clearance of the

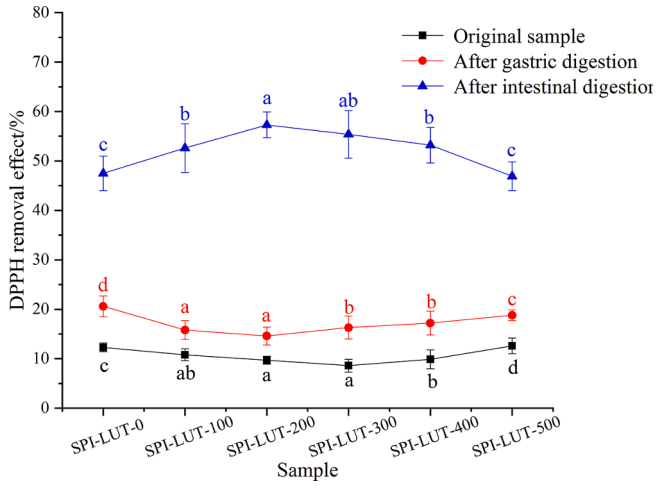

Fig. 14. DPPH clearance effect of the ultrasonically pretreated SPI-LUT nanodelivery system during gastrointestinal digestion.

nanodelivery system decreased first and then increased, which was consistent with the EE results. This shows that SPI of appropriate ultrasonic pretreatment could better embed LUT to reduce the DPPH clearance of the nanodelivery system. After intestinal digestion, the DPPH clearance rate of the sample continued to increase. This shows that in the gastric digestion stage, a portion of LUT was released, and the released LUT could scavenge free radicals, form more stable products and terminate the free radical chain reaction, which improved DPPH clearance [48]. When the SPI-LUT nanodelivery system was digested in the intestine, a large amount of LUT was released. This might be because the interaction between SPI and LUT altered the secondary protein structure and increased the number of binding sites with digestive enzymes, which improved the digestibility of protein and promoted the release of LUT[28]. Thus, the DPPH clearance of the SPI-LUT nanodelivery system was greatly improved. With the increase of ultrasound pretreatment power, the DPPH clearance of the nanodelivery system first increased (55.63 %) and then decreased. This is consistent with the EE results and simulated digestion in vitro. This indicates that appropriate ultrasound pretreatment power could increase the antioxidant activity of the nanodelivery system, which is related to the fact that ultrasound promotes the binding and release of SPI and more LUT.

4. Conclusion

Ultrasonic pretreatment of SPI facilitated the non-covalent complexation of SPI with LUT, leading to a higher encapsulation efficacy, loading amount, surface charge, and lower particle size and surface hydrophobicity of the SPI–LUT nanodelivery system. The ultrasonically pretreated SPI–LUT nanodelivery system exhibited flexible secondary structures and incompact tertiary conformations. The nanodelivery system treated with 200 W ultrasound exhibited the highest release rate of LUT and antioxidant activities. Appropriate ultrasonic pretreatment of SPI could better protect LUT from degradation caused by gastric acid corrosion and promote its massive release in SIF to improve the bioavailability and antioxidant activity of LUT. The improvement in these functional properties by the appropriate ultrasonic treatment could relate to stronger SPI–LUT interactions and structural modifications of the nanodelivery system. This study provides a preliminary basis for the expansion of the application field of soybean protein isolate and the efficient application of flavonoids.

CRediT authorship contribution statement

Fuwei Sun: Conceptualization, Software, Writing – original draft. **Bailiang Li:** Data curation. **Yanan Guo:** Methodology. **Yichang Wang:** Visualization. **Tianfu Cheng:** Investigation. **Qingyu Yang:** Supervision. **Jun Liu:** Supervision. **Zhijun Fan:** Supervision. **Zengwang Guo:** Funding acquisition, Project administration. **Zhongjiang Wang:** Writing – original draft, Conceptualization.

Declaration of Competing Interest

The authors declare that they have no known competing financial interests or personal relationships that could have appeared to influence the work reported in this paper.

Funding

Grants from the National key R&D plan in the 14th five year plan (2021YFD2100400), Heilongjiang Province “Hundred, Thousand, Ten Thousand” Engineering Science and Technology Major Project (2021ZX12B02), Shandong key R&D plan (major scientific and technological innovation project) (2022CXGC010603),Youth talent promotion project of China Association for science and technology (YESS20200271), Key R&D projects in Heilongjiang Province (GY2021ZB0204), The Special Fund of Liaoning Provincial Universities’ Fundamental Scientific Research Projects (LZD202002), Transformation project of major scientific and technological achievements in Heilongjiang Province (CG19A002), the Major industrial key projects for the transformation of new and old kinetic energy in Shandong Province funded this research.

References

[1] S. Achat, N. Rakotomanomana, K. Madani, O. Dangles, Antioxidant activity of olive phenols and other dietary phenols in model gastric conditions: Scavenging of the free radical DPPH and inhibition of the haem-induced peroxidation of linoleic acid, Food Chemistry 213 (15) (2016) 135–142.
[2] C. Arzeni, K. Martínez, P. Zema, A. Arias, A. Pérez, O.E. Pilosof, Comparative study of high intensity ultrasound effects on food proteins functionality, Journal of Food Engineering 108 (3) (2012) 463–472.
[3] D.F. Birt, S. Hendrich, W. Wang, Dietary agents in cancer prevention: flavonoids and isoflavonoids, Pharmacology & Therapeutics 90 (2–3) (2001) 157–177.
[4] M.M. Bradford, A rapid and sensitive method for the quantitation of microgram quantities of protein utilizing the principle of protein-dye binding, Analytical Biochemistry 72 (1–2) (1976) 248–254.
[5] F. Chen, B. Li, C. Tang, Nanocomplexation of soy protein isolate with curcumin: Influence of ultrasonic treatment, Food Research International 75 (2015) 157–165.
[6] W. Chen, R. Lv, A.I. Muhammad, M. Guo, T. Ding, X. Ye, D. Liu, Fabrication of (-)-epigallocatechin-3-gallate carrier based on glycosylated whey protein isolate obtained by ultrasound Maillard reaction, Ultrasonics Sonochemistry 58 (2019) 104678.
[7] W. Chen, X. Ma, W. Wang, R. Lv, M. Guo, T. Ding, X. Ye, S. Miao, D. Liu, Preparation of modified whey protein isolate with gum acacia by ultrasound maillard reaction, Food Hydrocolloids 95 (2019) 298–307.
[8] Y. Chen, M. Ma, Foam and conformational changes of egg white as affected by ultrasonic pretreatment and phenolic binding at neutral pH, Food Hydrocolloids 102 (2019), 105568.
[9] A.B. Tomé Constantino, E.E. Garcia-Rojas, Modifications of physicochemical and functional properties of amaranth protein isolate (Amaranthus cruentus BRS Alegria) treated with high-intensity ultrasound, Journal of Cereal Science 95 (2020) 103076.
[10] L. Dai, R. Li, Y. Wei, C. Sun, L. Mao, Y. Gao, Fabrication of zein and rhamnolipid complex nanoparticles to enhance the stability and invitro release of curcumin, Food Hydrocolloids 77 (2018) 617–628.
[11] T. Dai, R. Li, C. Liu, W. Liu, T.i. Li, J. Chen, M. Kharat, D.J. McClements, Effect of rice glutelin-resveratrol interactions on the formation and stability of emulsions: A multiphotonic spectroscopy and molecular docking study, Food Hydrocolloids 97 (2019) 105234.
[12] T. Dai, T.i. Li, R. Li, H. Zhou, C. Liu, J. Chen, D.J. McClements, Utilization of plant-based protein-polyphenol complexes to form and stabilize emulsions: Pea proteins and grape seed proanthocyanidins, Food Chemistry 329 (2020) 127219.
[13] H. Danafar, A. Sharafi, H. Kheiri Manjili, S. Andalib, Sulforaphane delivery using mPEG–PCL co-polymer nanoparticles to breast cancer cells, Pharmaceutical Development & Technology 22 (5) (2017) 642–651.
[14] H. Dang, M. Meng, H. Zhao, J. Iqbal, R. Dai, Y. Deng, F. Lv, Luteolin-loaded solid lipid nanoparticles synthesis, characterization, & improvement of bioavailability, pharmacokinetics in vitro and vivo studies, Journal of Nanoparticle Research 16 (4) (2014) 2347.
[15] Q. Du, Y. Wu, S. Tang, M. Ren, Z. Fu, Influences of ultrasonic treatment on structure and functional properties of salt:oluble protein from Moringa oleifera

seeds, International Journal of Food Science & Technology 56 (11) (2021) 5871–5880.
[16] Z. Fang, X. Cai, J. Wu, L. Zhang, Y. Fang, S. Wang, Effect of simultaneous treatment combining ultrasonication and pH-shifting on SPI in the formation of nanoparticles and encapsulating resveratrol, Food Hydrocolloids 111 (2021), 106250.
[17] K. Gao, F. Zha, Z. Yang, J. Rao, B. Chen, Structure characteristics and functionality of water-soluble fraction from high-intensity ultrasound treated pea protein isolate, Food Hydrocolloids 125 (2021), 107409.
[18] M. Geng, Z. Wang, L. Qin, A. Taha, L. Du, X. Xu, S. Pan, H. Hu, Effect of ultrasound and coagulant types on properties of β-carotene bulk emulsion gels stabilized by soy protein, Food Hydrocolloids 123 (2022) 107146.
[19] S.S. Gupta, M. Ghosh, Octacosanol educes physico-chemical attributes, release and bioavailability as modified nanocrystals, European Journal of Pharmaceutics and Biophar- maceutics 119 (2017) 201–214.
[20] L. Hao, J. Sun, M. Pei, G. Zhang, C. Li, C. Li, X. Ma, S. He, L. Liu, Impact of non-covalent bound polyphenols on conformational, functional properties and in vitro digestibility of pea protein, Food Chemistry 383 (2022) 132623.
[21] J.B. Harbone, C.A. Williams, ChemInform Abstract: Advances in Flavonoid Research Since 1992, ChemInform 32 (7) (2001) 481–504.
[22] W. He, H. Mu, Z. Liu, M. Lu, F. Hang, J. Chen, M. Zeng, F. Qin, Z. He, Effect of preheat treatment of milk proteins on their interactions with cyanidin-3-O-glucoside, Food Research International 107 (2018) 394–405.
[23] H. Hu, J. Wu, E.C.Y. Li-Chan, L. Zhu, F. Zhang, X. Xu, G. Fan, L. Wang, X. Huang, S. Pan, Effects of ultrasound on structural and physical properties of soy protein isolate (SPI) dispersions, Food Hydrocolloids 33 (2) (2013) 647–655.
[24] L. Huang, X. Ding, C. Dai, H. Ma, Changes in the structure and dissociation of soybean protein isolate induced by ultrasound-assisted acid pretreatment, Food Chemistry 232 (2017) 727–732.
[25] M. Imran, A. Rauf, T. Abu-Izneid, M. Nadeem, M.S. Mubarak, Luteolin, a flavonoid, as an anticancer agent: A review, Biomedicine & Pharmacotherapy 112 (2020), 108612.
[26] M. Jackson, H.H. Mantsch, The Use and Misuse of FTIR Spectroscopy in the Determination of Protein Structure, Critical Reviews in Biochemistry and Molecular Biology 30 (2) (1995) 95–120.
[27] L. Jiang, J. Wang, Y. Li, Z. Wang, J. Liang, R. Wang, Y. Chen, W. Ma, B. Qi, M. Zhang, Effects of ultrasound on the structure and physical properties of black bean protein isolates, Food Research International 62 (2014) 595–601.
[28] L. Lin, M. Jiao, M. Zhao, W. Sun, In vitro gastrointestinal digest of catechin-modified β-conglycinin oxidized by lipoxygenase-catalyzed linoleic acid peroxidation, Food Chemistry 280 (2019) 154–163.
[29] I.J. Joye, G. Davidov-Pardo, R.D. Ludescher, D. Mcclements, Fluorescence quenching study of resveratrol binding to zein and gliadin: Towards a more rational approach to resveratrol encapsulation using water-insoluble proteins, Food Chemistry 185 (2015) 261–267.
[30] Khan, J., Alexander, A., Ajazuddin, Saraf, S., & Saraf, S. (2015). LuteolinÎ Çôphospholipid complex: preparation, characterization and biological evaluation. *Journal of Pharmacy & Pharmacology. 66*(10). 1451-1462.
[31] J.R. Lakowicz, G.J.B. Weber, Quenching of protein fluorescence by oxygen. Detection of structural fluctuations in proteins on the nanosecond time scale, Biochemistry 12 (21) (1973) 4171–4179.
[32] T. Lan, Y. Dong, M. Zheng, L. Jiang, Y. Zhang, X. Sui, Complexation between soy peptides and epigallocatechin-3-gallate (EGCG): Formation mechanism and morphological characterization, LWT – Food Science and Technology 134 (2020) 109990.
[33] Y. Li, Y.u. Cheng, Z. Zhang, Y. Wang, B.K. Mintah, M. Dabbour, H. Jiang, R. He, H. Ma, Modification of Rapeseed Protein by Ultrasound-assisted pH Shift Treatment: Ultrasonic Mode and Frequency Screening, Changes in Protein Solubility and Structural Characteristics, Ultrasonics Sonochemistry 69 (2020) 105240.
[34] F. Liu, C. Ma, D.J. Mcclements, Y. Gao, A comparative study of covalent and non-covalent interactions between zein and polyphenols in ethanol-water solution, Food Hydrocolloids 63 (2017) 625–634.
[35] Z. Ma, L. Li, C. Wu, Y. Huang, F. Teng, Y. Li, Effects of combined enzymatic and ultrasonic treatments on the structure and gel properties of soybean protein isolate, LWT – Food Science and Technology 158 (2022) 113123.
[36] F. Mehranfar, A.-K. Bordbar, H. Parastar, A combined spectroscopic, molecular docking and molecular dynamic simulation study on the interaction of quercetin with β-casein nanoparticles, Journal of Photochemistry & Photobiology, B: Biology 127 (5) (2013) 100–107.
[37] O. Menéndez-Aguirre, A. Kessler, W. Stuetz, T. Grune, J. Weiss, J. Hinrichs, Increased loading of vitamin D2 in reassembled casein micelles with temperature-modulated high pressure treatment, Food Research International 64 (2014) 74–80.
[38] D. Meng, L. Zhu, L. Zhang, T. Ma, Y. Zhang, L. Chen, Y. Shan, Y. Wang, Z. Wang, Z. Zhou, R. Yang, Succinylated ferritin as a novel nanocage-like vehicle of polyphenol: structure, stability, and absorption analysis, Food Chemistry 361 (2021) 130069.
[39] M. Minekus, M. Alminger, P. Alvito, S. Ballance, T. Bohn, C. Bourlieu, F. Carrière, R. Boutrou, M. Corredig, D. Dupont, C. Dufour, L. Egger, M. Golding, S. Karakaya, B. Kirkhus, S. Le Feunteun, U. Lesmes, A. Macierzanka, A. Mackie, S. Marze, D. J. McClements, O. Ménard, I. Recio, C.N. Santos, R.P. Singh, G.E. Vegarud, M.S. J. Wickham, W. Weitschies, A. Brodkorb, A standardised static in-vitro digestion method suitable for food – an international consensus, Food & Function 5 (6) (2014) 1113–1124.
[40] Morales, R., Martínez, K. D., Ruiz-Henestrosa, Victor. M. P., & Pilosof, A. M. R. (2015). Modification of foaming properties of soy protein isolate by high ultrasound intensity: Particle size effect. *Ultrasonics – Sonochemistry. 26*. 48-55.
[41] K. Mougin, A. Bruntz, D. Severin, A. Teleki, Morphological stability of microencapsulated vitamin formulations by AFM imaging, Food Structure 9 (2016) 1–12.
[42] W. Ning, X. Zhou, W. Wang, L. Wang, L. Jiang, T. Liu, D. Yu, Effect of high intensity ultrasound on the structure and solubility of soy protein isolate-pectin complex, Ultrasonics Sonochemistry 80 (2021), 105808.
[43] T.B. Pessato, F.P.R. de Morais, N.C. de Carvalho, A.C.M. Figueira, L.G. R. Fernandes, R.d.L. Zollner, F.M. Netto, Protein structure modification and allergenic properties of whey proteins upon interaction with tea and coffee phenolic compounds, Journal of Functional Foods 51 (2018) 121–129.
[44] W. Qing, Y. Wang, H. Li, F. Ma, J. Zhu, X. Liu, Preparation and Characterization of Copolymer Micelles for the Solubilization and In Vitro Release of Luteolin and Luteoloside, Aaps Pharmscitech 18 (6) (2017) 2095–2101.
[45] K. Rao, M. Imran, T. Jabri, I. Ali, S. Perveen, Shafiullah, S. Ahmed, M.R. Shah, Gum tragacanth stabilized green gold nanoparticles as cargos for Naringin loading: A morphological investigation through AFM, Carbohydrate Polymers 174 (2017) 243–252.
[46] H.H.F. Refsgaard, L. Tsai, E.R. Stadtman, Modifications of proteins by polyunsaturated fatty acid peroxidation products, Proceedings of the National Academy of Sciences of the United States of America 97 (2) (2000) 611–616.
[47] N. Shahabadi, M. Maghsudi, Z. Kiani, M. Pourfoulad, Multispectroscopic studies on the interaction of 2-tert-butylhydroquinone (TBHQ), a food additive, with bovine serum albumin, Food Chemistry 124 (3) (2011) 1063–1068.
[48] A. Shirwaikar, A. Shirwaikar, K. Rajendran, I. Punitha, In vitro antioxidant studies on the benzyl tetra isoquinoline alkaloid berberine, Biological & Pharmaceutical Bulletin 29 (9) (2006) 1906–1910.
[49] X. Sui, H. Sun, B. Qi, M. Zhang, Y. Li, L. Jiang, Functional and conformational changes to soy proteins accompanying anthocyanins: Focus on covalent and non-covalent interactions, Food Chemistry 245 (2018) 871–878.
[50] A. Taha, E. Ahmed, A. Ismaiel, M. Ashokkumar, X. Xu, S. Pan, H. Hu, Ultrasonic emulsification: An overview on the preparation of different emulsifiers-stabilized emulsions, Trends in Food Science & Technology 105 (2020) 363–377.
[51] Z. Wan, L. Wang, X. Yang, J. Wang, L. Wang, Controlled formation and stabilization of nanosized colloidal suspensions by combination of soy protein and biosurfactant stevioside as stabilizers, Food Hydrocolloids 52 (2016) 317–328.
[52] W. Xia, H. Zhang, J. Chen, H. Hu, F. Rasulov, D. Bi, X. Huang, S. Pan, Formation of amyloid fibrils from soy protein hydrolysate: Effects of selective proteolysis on β-conglycinin, Food Research International 100 (2017) 268–276.
[53] J. Xu, M. Hao, Q. Sun, L. Tang, Comparative studies of interaction of β-lactoglobulin with three polyphenols, International Journal of Biological Macromolecules 136 (2019) 804–812.
[54] H. Xue, G. Zhang, T. Han, R. Li, H. Liu, B. Gao, Y. Tu, Y. Zhao, Improvement of gel properties and digestibility of the water-soluble polymer of tea polyphenol-egg white under thermal treatment, Food Chemistry 372 (2022) 131319.
[55] S. Yan, F. Xie, S. Zhang, L. Jiang, B. Qi, Y. Li, Effects of soybean protein isolate polyphenol conjugate formation on the protein structure and emulsifying properties: Protein polyphenol emulsification performance in the presence of chitosan, Colloids and Surfaces A: Physicochemical and Engineering Aspects 609 (2020), 125641.
[56] S. Yan, J. Xu, S. Zhang, Y. Li, Effects of flexibility and surface hydrophobicity on emulsifying properties: Ultrasound-treated soybean protein isolate, LWT – Food Science and Technology 142 (2021) 110881.
[57] G. Yen, J. Wu, Antioxidant and radical scavenging properties of extracts from Ganoderma tsugae, Food Chemistry 65 (3) (1999) 375–379.
[58] Y. Zhang, S. Chen, B. Qi, X. Sui, L. Jiang, Complexation of thermally-denatured soybean protein isolate with anthocyanins and its effect on the protein structure and in vitro digestibility, Food Research International 106 (2018) 619–625.
[59] Q. Zhang, Z. Cheng, Y. Wang, L. Fu, Dietary protein-phenolic interactions: characterization, biochemical-physiological consequences, and potential food applications, Critical Reviews in Food Science and Nutrition 61 (21) (2021) 3589–3615.
[60] Y. Zhang, Q. Zhong, Effects of thermal denaturation on binding between bixin and whey protein, Journal of Agricultural and Food Chemistry 60 (30) (2012) 7526–7531.
[61] Q. Zhao, T. Xie, X. Hong, Y. Zhou, L. Fan, Y. Liu, J. Li, Modification of functional properties of perilla protein isolate by high-intensity ultrasonic treatment and the stability of o/w emulsion, Food Chemistry 368 (2021), 130848.
[62] P. Zhu, L. Chen, Y. Zhao, C. Gao, J. Yang, X. Liao, D. Liu, B.o. Yang, A novel host-guest complex based on biotin functionalized polyamine-β-cyclodextrin for tumor targeted delivery of luteolin, Journal of Molecular Structure 1237 (2021) 130339.